

# Fabrication And Characterization Of P-Mns:0.01Al/N-Si Heterojunction For Photodiode Application

Alia A. Shehab

Suha. A. Fadaam

Collage of Education for pure science, Ibn Al-Haitham University of Baghdad, Baghdad, Iraq

Corresponding author: [ahmed\\_naji\\_abd@yahoo.com](mailto:ahmed_naji_abd@yahoo.com)

**Abstract**—In this study, P-MnS:Al/n-Si has been fabricated by high vacuum thermal evaporation. Structural , morp-hology and optical of MnS:Al has been investigated . XRD measurements disclosed that the MnS was cubic crystal structure. AFM imag showed that the produced MnS films have semi spherical shaped with a high homoge-nous . The energy band gap of MnS:Al films which prepared by thermal evaporation technique has been deter-mined from optical measurements found to be around (2.97) eV. Dark and illuminated current-voltage I-V characteristics, spectral responsivity ,specific detectivity , and minority carrier lifetime of photodiode relive that the MnS:Al can be used as a photodiode application .

**Keywords**—MnS:Al thin film , Respo-nsivity ,Detectivity.

## 1. Introduction:

Recently metal chalcogenide thin film materials have opened a new area in The field of electronic applications. Their properties can be changed by changing the crystallite size and/or thickness of the film depending upon the deposition conditions, the structural ,electrical and optical properties of these materials can be controlled in many ways [1–5] Materials containing manganese are interesting because their applications are possible in many areas of modern technology.

Manganese sulfide MnS is a magnetic semiconductor material ( $E_g=3.1\text{eV}$ ) that is of potential interest in short wavelength optoelectronic applications such as in solar selective coatings, solar cells, sensors, photoconductors, optical mass memories [6–9]. MnS thin films or powders can be found in several polymorphic forms: the rock salt type structure ( $\alpha$ -MnS) .which is the most common form, by low temperature growing techniques it crystallizes into the zinc blende ( $\beta$ -MnS) or wurtzite ( $\gamma$ -MnS) structure [10,11].

MnS is extensively studied in the literature, preparation of its thin films has been carried out by different metho-ds such as radiofrequency sputtering [12,13],hydrothermal[14-16] ,molecular beam epitaxy [17] and chemical bath deposition (CBD) [9,18] The properties of thin films prepared by different methods are critically dependent on the nature of preparation technique

## 2. Experimental work.

The films of Manganese Sulfide doped with aluminum were prepared by thermal evaporation technique using coating unit in a vacuum about  $2 \times 10^{-5}$  Torr. A specific weight from Manganese Sulfide powder (99.9% pure) must be taken and put it in a special evaporation

molybdenum boat, after evaporation Manganese Sulfide thin films we take ratio (1%) from this weight from Aluminum and put it in other molybdenum boat. We used thermal diffusion method to doped Manganese Sulfide thin films with Aluminum, Glass and silicon wafer was used as substrate materials for the deposition of MnS:Al thin films. Glass slides were cut into (1.5×1.5) cm compatible with the dimension of substrate holder by using a steel cutter tool. The glass slides were thoroughly cleaned before the deposition process in to attain a plausible adhesion coefficient as in the following procedure. The glass slides were first cleaned with a dilute solution of chemical detergent to remove the impurities and the protein materials on the surface of the slides. Then Si samples were cleaned with alcohol and an ultrasonic bath in order to remove the impurities and residuals from their surface. These substrates were etched with HF (10%) for 5 min to remove the native oxide. The rate of evaporation was (23.5 nm/min) and the film thickness (400±10nm) was measured by interference method. The substrate glass was placed directly above the source at a distance about 18 cm after cleaned the glass and the this film which deposited one study the structural, topography and optical properties of films MnS:AL were investigated separately by means of (CuK $\alpha$ ) XRD-6000, Shimadzu X-ray diffractometer, Fourier transform-infrared spectroscopy, JEOL (JSM-5600) scanning electron microscopy, Philips CM10 pw 6020 transmission electron microscopy, Angstrom AA 3000 Atomic Fourier transformation

infrared spectroscopy (FTIR- 8400S) and Cary 100 Conc plus UV-Vis spectrophotometer.

### 3. Results and discussion

Figure (1) shows the XRD different pattern of (MnS:Al) which prepped thin films by thermal evaporation technique and deposited on glass substrate. The figure (1) reveals contain three peaks at diffraction angle of 29.94°, 34.45° and 49.28° corresponding to (111), (200) and (220) and planes which have been compared with standard XRD diffraction data file (ASTM NO 06-0518). All the diffraction peaks in figure (1) are indicates to cubic structure with no trail of hexagonal or other faces.

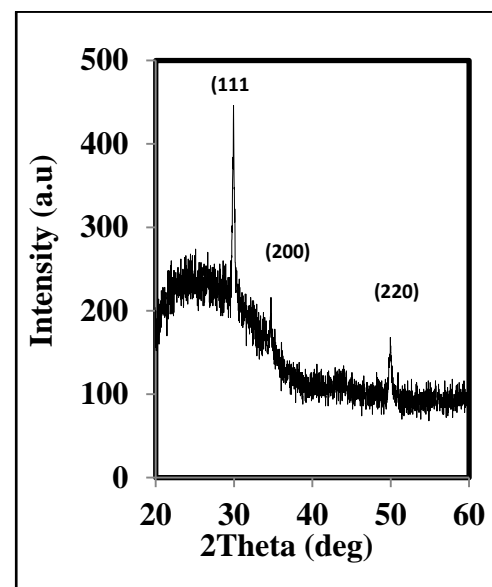


*Fig. (2): XRD spectra of MnS:Al films deposited as prepped.*

The crystallite size was calculated by using Debye-Scherrer's relation [19]:

$$G_s = \frac{0.9 \lambda}{\beta \cos \theta} \quad (1)$$

Where  $G_s$  is the crystallite size,  $\beta$  the full width at half maxima,  $\theta$  is the angle of diffraction, and  $\lambda$  is the wave-length of X-ray.

The strain value  $\eta$  and the dislocation density  $\delta$  value can be evaluated by using the relations in equation 2 and 3 [2], see Table (1):

$$\eta = \frac{\beta \cos \theta}{4} \quad (2)$$

$$\delta = \frac{1}{G_s^2} \quad (3)$$

**Table (1) crystallite size, strain and dislocation density for MnS:Al thin films**

Sample	$G_s(\text{nm})$	$\eta * 10^{-4}$ (lines.m <sup>-2</sup> )	$\delta * 10^{15}$ (lines.m <sup>-2</sup> )
MnS:Al	10.02	4.56	9.49

Figure (2) shows 3D AFM image and Granularity accumulation distribution chart of MnS:Al nanostructure prepared by thermal evaporation technique and deposited on glass. Substrate is well covered with MnS:Al nanostructure; distributed uniformly on the surface. The Table (2), it is clearly seen that the root mean square of surface roughness.

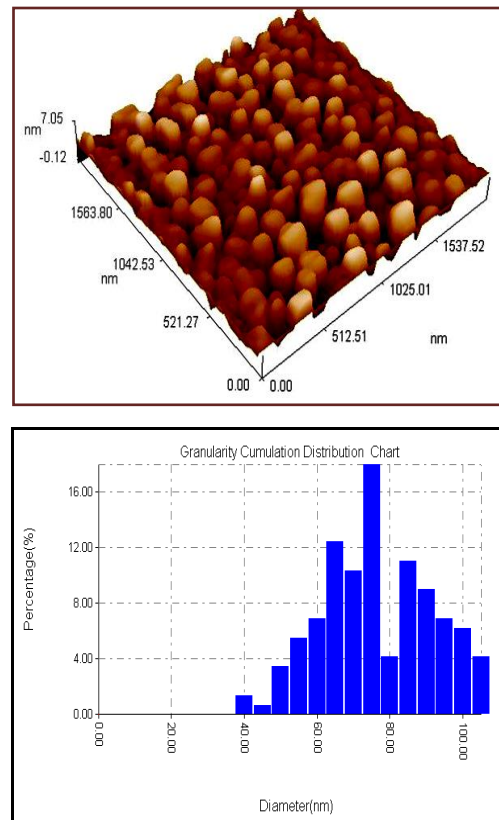
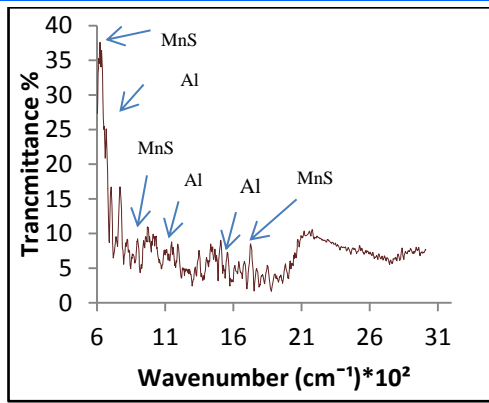


**Fig 2: 3D AFM images of MnS:Al thin films surface and Granularity accumulation distribution chart .**

**Table (2): Average grain, Roughness density and RMS of MnS:Al thin films**

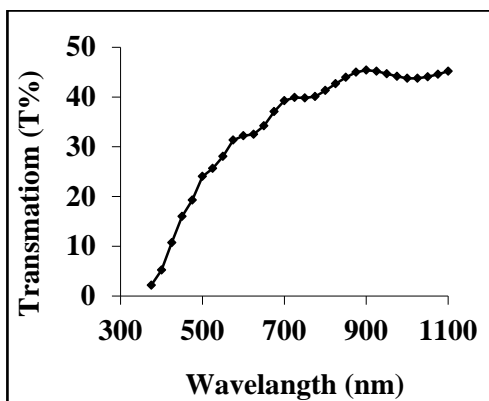
Sample	Average G.S(nm)	Roughness (nm)	R.M.S (nm)
MnS:Al	73.71	1.1	1.29

Figure (3) shows the FTIR spectra of MnS:Al Sample which showed several significant absorption peaks , The broad absorption band in the region of ( 600-2100) cm<sup>-1</sup> is assigned to MnS:Al stret-ching mode .The spectra of MnS showed the absorption bands at (624,897,1147 and 1732) cm<sup>-1</sup> in control and treated sample, attributing to –OH stretching vibration and spectra of Al showed the absorption bands at (667,1640, and1557) cm<sup>-1</sup> in control and treated sample, attributing to –OH stretching vibration.



**Fig. 3: FTIR spectra of MnS:Al thin films**

Figure (4) shows displays the tran-smission as a function of wavelength of MnS:Al thin films is which prepared by thermal evaporation techniques and dep-osited on glass substrate . It is obvious that the film gives good transparency characteristics at the spectral range (600- 1000) nm .The date is corrected for glass in UV-regain,the transmission is sharply increases because of the wide of absorbed particle size .Also the figure (3), the maximum value of transmittance (45.18 nm)



**Fig.4: Optical transmittance of MnS:Al thin films**

The optical energy gap of MnS was calculated by the relation [9]

$$\alpha h\nu = A(h\nu - E_g)^n \quad (4)$$

Where  $A$  is a constant,  $\nu$  is the transition frequency and the exponent  $n$  characterizes the nature of band transition.  $n = 1/2$  and  $3/2$  corresponds to direct allowed and direct forbidden transitions and  $n = 2$  and  $3$  corresponds to indirect allowed and indirect forbidden transitions, respectively. Figure (5) shows the band gap of MnS:Al thin films is which prepared by thermal evaporation techniques and deposited on glass substrate. measured from the plot of the square of  $(\alpha h\nu)^2$  versus photon energy  $h\nu$  (where  $\alpha$  is the absorption coefficient) by extrapo-lating the linear part of the curve toward the photon energy axis. The optical energy gap of MnS:Al is found to be (2.97) eV, [18]

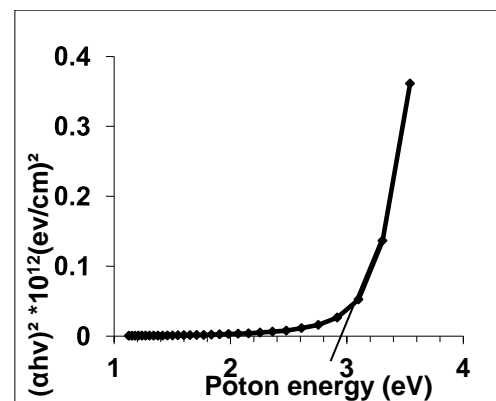


**Fig. 5: Plot of  $(\alpha h\nu)^2$  versus  $h\nu$  curve of as-prepared MnS:Al**

Figure (6) show the I-V dark characteristics in forward and reverse direction of Al/MnS:Al/Si/Al hetero-junction. The forward current of hetrojunction is very small at voltage less than (1) V . The current is known as

recombination current which occurs at low voltages only. It is generated when each electron excited from valence band to conductive band. The second region at high voltage represented the diffusion or bending region, which depending on series resistance. In this region; the bias voltage can deliver electrons with enough energy to penetrate the barrier between the two sides of the junction.

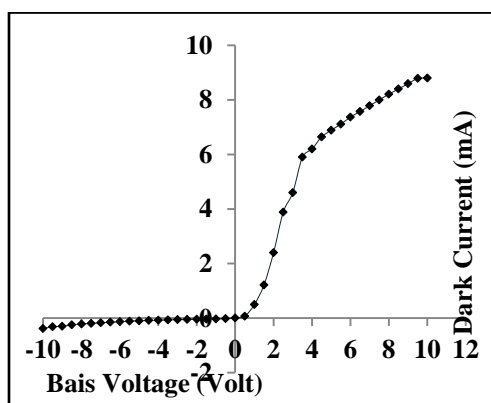


Fig.6.I-V characteristic of the MnS:Al/Si

Figure 7 shows that the reversed current-voltage characteristics of the device measured in the photocurrent under (26.6, 14.4, 14.2) mW/cm tungsten lamp illuminations. It can be seen that the reverse current value at a given voltage for MnS:Al/Si heterodiode under illumination is higher than that in the dark and it can be seen from these figures that the current value at a given voltage for heterojunction under illumination is higher than that in dark, this indicates that the light generated carrier contributing photocurrent due to the production of electron-hole as a result of the light absorption. This behavior yields useful information on the electron-hole pairs,

which are effectively generated in the junction by incident photons

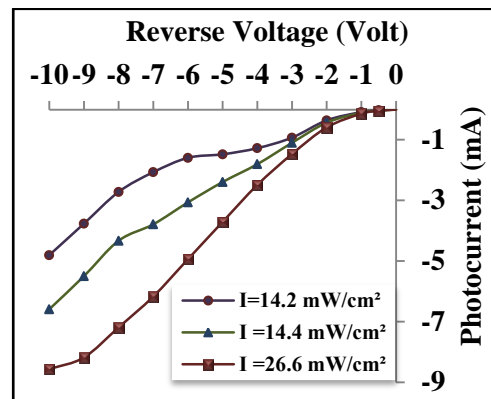


Fig.7.I-V characteristic under forward reverse bias of the MnS:Al/Si

Figure (8) shows a linear relation between the inverse of the square of capacitance ( $1/C^2$ ) versus reverse bias voltage for MnS:Al/Si, indicating an abrupt junction. The built-in potential  $V_b$  value was obtained after extrapolating the ( $1/C^2$ ) point to the voltage axis. The built-in potential  $V_b$  for MnS:Al/Si was 1.05 volt.

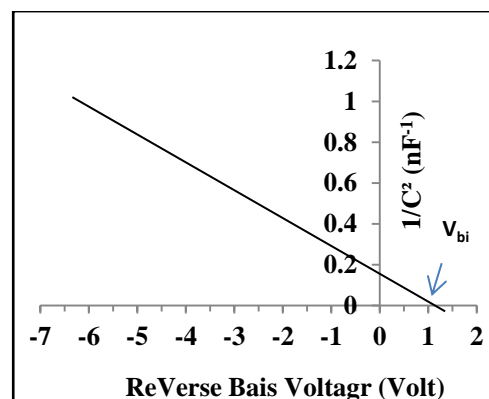
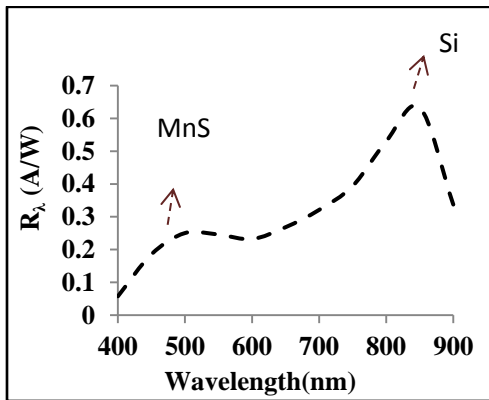


Fig. 8:  $1/C^2$  versus reverse voltage of MnS:Al/Si photodiodes

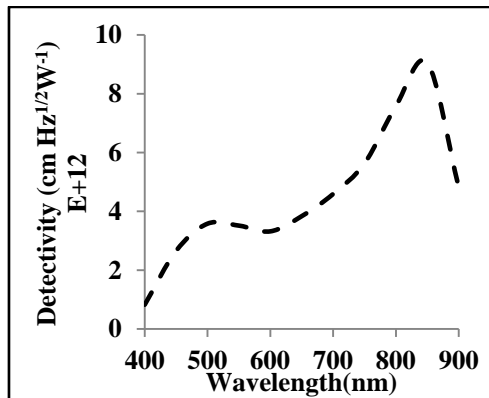
Figure (9) shows that the spectral responsivity curve of MnS:Al/Si consists of two peaks of response; the first peak is located at  $500 \pm 50$  nm due to the absorption edge of MnS:Al/Si

nanoparticles, while the second region is located at  $800 \pm 50$  nm due to absorption edge of silicon.



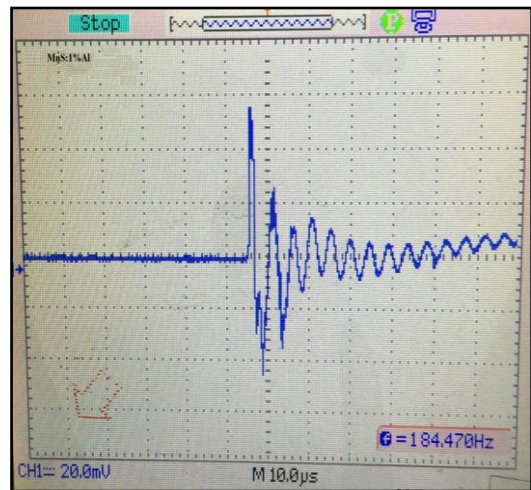
**Fig.9. Spectral responsivity as a function of wavelength of MnS:Al/Si photodiode**

Figure 10 shows spectral detectivity as a function of wavelength (400 nm-900 nm). This figure shows that it is dependent directly on the spectral responsivity.



**Fig.10: Spectral detectivity as a function of wavelength of MnS:Al/Si photodiode**

Figure (11) shows that the best photodetectors have a lifetime of 10 μsec.



**Fig. 10. Images for Lifetime heterojunction MnS:Al/Si**

### Conclusion

The MnS:Al/Si heterojunction was successfully fabricated by using the thermal evaporation technique. MnS:Al shows good transparency in the spectral range (400-900) nm, and the electrical characteristics of the heterojunction are strongly dependent on the structure. The maximum value of spectral responsivity  $R_{\lambda}$  of MnS:Al photodetector is around 0.25 A/W at  $\approx 500 \pm 50$  nm. The maximum value of the specific detectivity  $D_{\lambda}$  is found to be  $3.580 \times 10^{12} \text{ W}^{-1} \cdot \text{cm} \cdot \text{Hz}^{-1}$  located at  $500 \pm 50$  nm wavelength for MnS:Al/Si photodetector.

### References

- [1] L. Eckertova, Physics of Thin Films Processes, Plenum Press, New York NY, 1986.
- [2] C.D. Lokhande, Mater. Chem. Physics, 27, (1991) 1.
- [3] R.N. Bhattacharya, J. Electrochem. Soc. 129 (1992) 332.

- [4] R.L. Greene, D.D. Sell, Phys. Rev. 171 (1968) 600.
- [5] P. O'Brien, D.-J. Otway, D.S. Boyle, Thin Solid Films 361 (2000) 17.
- [6] D. Fan, X. Yang, H. Wang, Y. Zhang, H. Yan, Physica. B 337 (2003) 165.
- [7] B. Piriou, J.D. Ghys, S.Mochizuki, J. Phys., Condens. Matter 6 (1994) 7317.
- [8] R. Tappero, P. D'Arco, A. Lichanot, Chem. Phys. Lett. 273 (1997) 83.
- [9] C.D. Lokhande, A. Ennaoui, P.S. Patil, M. Giersig, M. Muller, K. Diesner, H. Tributsch, Thin Solid Films 330 (1998) 70.
- [10] R.L. Clendenen, H.G. Drickamer, J. Chem. Phys. 44 (1966) 4223.
- [11] M. Kobayashi, T. Nakai, S. Mochizuki, N. Takayama, J. Phys. Chem. Solids 56 (1995) 341.
- [12] S.A. Mayen-Hernandez, S.J. Sandoval, R.C. Perez, G.T. Delgado, B.S. Chao, O.J. Sandoval, J. Cryst. Growth 256 (2003) 12.
- [13] I. Oidor-Juarez, P. Jimenez, G.T. Delgado, R.C. Perez, O.J. Sandoval, B. Chao, S.J. Sandoval, Mater. Res. Bull. 37 (2002) 1749.
- [14] Y. Zhang, H. Wang, B. Wang, H. Yan, M. Yoshimura, J. Cryst. Growth 243 (2002) 214.
- [15] C. An, K. Tang, X. Liu, F. Li, G. Zhou, Y. Qian, J. Cryst. Growth 252 (2002) 575.
- [16] Y. Zhang, H. Wang, B. Wang, H. Xu, H. Yan, M. Yoshimura, Opt. Mater. 23 (2003) 433.
- [17] L. David, C. Bradford, X. Tang, T.C.M. Graham, K.A. Prior, B.C. Cavenett, J. Cryst. Growth 251 (2003) 591.
- [18] D. sreeantha .reddy ,D.raja .reddy,B.K.reddy .etc"Annealing effect on physical of thermally evaporated MnS nanocrystalline films ".Journal of optoelectronic and materials ,9,7 (2007)2019-2022.
- [19] B.D.Cuttity and S.R.Stock , Element of X-ray diffraction ,3<sup>rd</sup> Ed .(2001) .